HHS Public Access

Author manuscript

J Proteomics. Author manuscript; available in PMC 2021 March 22.

Published in final edited form as:

J Proteomics. 2018 October 30; 189: 48–59. doi:10.1016/j.jprot.2018.04.005.

Quantitative targeted proteomic analysis of potential markers of tyrosine kinase inhibitor (TKI) sensitivity in EGFR mutated lung adenocarcinoma

Shivangi Awasthi[a,c], **Tapan Maity**[a], **Benjamin L. Oyler**[b], **Yue Qi**[a], **Xu Zhang**[a], **David R. Goodlett**[c], **Udayan Guha**[a,*]

[a]Thoracic & Gastrointestinal Oncology Branch, Center for Cancer Research, NCI, Bethesda, MD, United States

[b]School of Medicine, University of Maryland, Baltimore, MD, United States

[c]School of Pharmacy, University of Maryland, Baltimore, MD, United States

Abstract

Lung cancer causes the highest mortality among all cancers. Patients harboring kinase domain mutations in the epidermal growth factor receptor (EGFR) respond to EGFR tyrosine kinase inhibitors (TKIs), however, acquired resistance always develops. Moreover, 30–40% of patients with EGFR mutations exhibit primary resistance. Hence, there is an unmet need for additional biomarkers of TKI sensitivity that complement EGFR mutation testing and predict treatment response. We previously identified phosphopeptides whose phosphorylation is inhibited upon treatment with EGFR TKIs, erlotinib and afatinib in TKI sensitive cells, but not in resistant cells. These phosphosites are potential biomarkers of TKI sensitivity. Here, we sought to develop modified immuno-multiple reaction monitoring (immuno-MRM)-based quantitation assays for select phosphosites including EGFR-pY1197, pY1172, pY998, AHNAK-pY160, pY715, DAPP1-pY139, CAV1-pY14, INPPL1-pY1135, NEDD9-pY164, NF1-pY2579, and STAT5A-pY694. These sites were significantly hypophosphorylated by erlotinib and a 3rd generation EGFR TKI, osimertinib, in TKI-sensitive H3255 cells, which harbor the TKI-sensitizing $EGFR^{L858R}$ mutation. However, in H1975 cells, which harbor the TKI-resistant $EGFR^{L858R/T790M}$ mutant, osimertinib, but not erlotinib, could significantly inhibit phosphorylation of EGFR-pY-1197, STAT5A-pY694 and CAV1-pY14, suggesting these sites also predict response in TKI-resistant cells. We could further validate EGFR-pY-1197 as a biomarker of TKI sensitivity by developing a calibration curve-based modified immuno-MRM assay.

Significance: In this report, we have shown the development and optimization of MRM assays coupled with global phosphotyrosine enrichment (modified immuno-MRM) for a list of 11 phosphotyrosine peptides. Our optimized assays identified the targets reproducibly in biological samples with good selectivity. We also developed and characterized quantitation methods to determine endogenous abundance of these targets and correlated the results of the relative

*Corresponding author at: Center for Cancer Research/NCI/NIH, 9000 Rockville Pike, Bethesda, MD 20892, United States. udayan.guha@nih.gov (U. Guha).

Supplementary data to this article can be found online at https://doi.org/10.1016/j.jprot.2018.04.005.

quantification with amounts estimated from the calibration curves. This approach represents a way to validate and verify biomarker candidates discovered from large-scale global phospho-proteomics analysis. The application of these modified immuno-MRM assays in lung adenocarcinoma cells provides proof-of concept for the feasibility of clinical applications. These assays may be used in prospective clinical studies of EGFR TKI treatment of EGFR mutant lung cancer to correlate treatment response and other clinical endpoints.

Keywords

MRM; EGFR; Lung cancer; Phosphoproteomics; Tyrosine kinase inhibitor; Targeted proteomics

1. Introduction

Lung cancer is a major public health problem and a leading cause of mortality in the United States for both men and women. It is estimated that there will be 222,500 new cases and 155,870 deaths from lung cancer in 2017 [1]. Non-small cell lung cancer (NSCLC) is the most common type of lung cancer and makes up 85% of all lung cancer diagnoses, with adenocarcinoma being the most common histology. Aberrant regulation of EGFR causes increased intracellular signaling through tyrosine kinase activation leading to cell growth, angiogenesis, inhibition of apoptosis, invasion and metastasis. Somatic mutations in the kinase domain of EGFR include a L858R point mutation in exon 21 [2] and exon 19 in-frame deletions, such as Del E746-A750 which collectively make-up over 90% of known activating EGFR mutations. Mutations in the kinase domain of EGFR provide sensitivity to EGFR-tyrosine kinase inhibitor (EGFR-TKI) therapy [3–5]. The first-generation EGFR-TKIs, erlotinib and gefitinib, and the second-generation TKI, afatinib, were approved by the FDA for front-line therapy to treat patients harboring kinase domain EGFR mutations [6–8]. Unfortunately, all patients developed secondary resistance to EGFR-TKIs within 9–14 months of treatment. Several mechanisms of development of acquired resistance have been elucidated. The most common acquired resistance mechanism that occurs in 50–60% of patients is the acquisition of a second site mutation at the gatekeeper site residue in exon 20, T790M [9,10]. Other mechanisms of resistance include MET amplification [11–13] and small cell lung cancer (SCLC) transformation [14,15]. However, in 20–25% of estimated cases, the mechanisms of acquired resistance to 1st and 2nd generation EGFR TKIs remain unknown. Moreover, approximately 30–40% of patients harboring TKI-sensitizing mutations exhibit intrinsic resistance to TKI treatment [16–18]. Therefore, it is essential to identify early treatment biomarkers and characterize the mechanisms of intrinsic and acquired resistance to EGFR TKIs to better guide the development of new drugs or combination strategies to help overcome TKI- resistance.

We have previously employed a liquid chromatography-tandem mass spectrometry (LC MS/MS) shotgun phosphoproteomics approach that used stable isotope labeling with amino acids in cell culture (SILAC) to identify novel targets of mutant EGFR signaling in isogenic human bronchial epithelial cells [19], to characterize global phosphorylation (pSTY) changes upon immediate ligand stimulation, with or without prior 1st-generation EGFR TKI, erlotinib treatment [20], and to investigate the effect of erlotinib and 2nd generation EGFR TKI, afatinib on downstream tyrosine phosphorylation of several drug-sensitive and -

resistant human lung adenocarcinoma cell lines [21]. These studies showed that the degree of inhibition of tyrosine phosphorylation on several phosphosites correlates well with the extent of TKI-sensitivity. We have identified several tyrosine phosphorylation sites downstream of mutant EGFRs that are hyperphosphorylated in cells expressing mutant EGFRs, compared to those expressing wild type EGFR, and phosphorylation targets that are inhibited by EGFR TKIs, such as erlotinib and afatinib, in TKI sensitive cells, but not in resistant cells, suggesting these are potential biomarkers of TKI sensitivity. Here, we sought to develop multiple reaction monitoring (MRM) quantitation assays for a subset of candidate phosphopeptides from downstream protein targets of mutant EGFRs based on the above criteria. A previous study has shown the feasibility of MRM assays to reproducibly quantify temporal tyrosine phosphorylation profiles upon EGF stimulation in EGFR signaling [22]. Another study has shown utilization of quantitative targeted proteomics to monitor phosphorylation dynamics of the PI3K-mTOR and MAPK signaling pathways [23]. Development of sensitive MRM assays (especially for posttranslational modifications like phosphorylation) that detect low amounts of endogenous peptides in complex biological matrices usually involves incorporation of an additional enrichment step through an anti-peptide antibody [24,25]. The multiplexed immuno-MRM assays (peptide immunoaffinity enrichment coupled to MRM) have been utilized previously to investigate phospho-signaling in the DNA damage response network [26].

In this study, we developed modified immuno-MRM assays for a subset of tyrosine phosphorylated peptides (Table 1) and measured their basal phosphorylation levels in the 1st/2nd generation EGFR TKI-sensitive H3255 lung adenocarcinoma cell line, harboring the $EGFR^{L858R}$ mutation, and TKI–resistant cell line H1975, harboring the $EGFR^{L858R/T790M}$ mutation, and compared that to phosphorylation levels after treatment with the 1st generation EGFR TKI, erlotinib, and the 3rd generation EGFR TKI, osimertinib. 3rd generation EGFR TKIs, such as osimertinib can circumvent resistance to 1st and 2nd generation EGFR TKIs resulting from the acquisition of the $EGFR^{T790M}$ mutation [27]. Based on our previously published global phosphoproteomics studies, we hypothesized that these phosphotyrosine sites are the markers of sensitivity to EGFR TKIs. To test this hypothesis, we quantified the degree of tyrosine phosphorylation of these sites in 1st and 2nd generation EGFR TKI-sensitive and -resistant cells upon treatment with erlotinib or osimertinib. We show that phosphorylation of all these sites were inhibited by EGFR TKIs in H3255 cells, while in H1975 cells, EGFR-pY1197, STAT5A-pY694 and CAV1-pY14 were significantly inhibited by osimertinib, but not erlotinib using relative quantitation. Results of quantitation using calibration curves could validate EGFR-pY1197 as a potential biomarker of TKI sensitivity, regardless of the TKI used.

2. Materials and methods

2.1. Cell culture and lysate preparation

The two lung adenocarcinoma cell lines used in this study were H3255, harboring the EGFR L858R mutation, and H1975, harboring both EGFR L858R and T790M mutations. H1975 was purchased from American Type Culture Collection (ATCC) and H3255 was a kind gift from Dr. Bruce Johnson. These cells were cultured in RPMI media 1640 (Thermo Scientific,

San Jose, CA) containing 10% dialyzed fetal bovine serum (Invitrogen, Carlsbad, CA) and 1% penicillin/streptomycin. The cells were grown in several 15 cm dishes (2–3 × 10^7 cells/dish) at 37 °C, 5% CO_2 and high humidity. H3255 and H1975 cells were treated with DMSO (vehicle), and EGFR TKIs, erlotinib and osimertinib (both prepared in the vehicle) at 100 nM for 1 h. Following treatment, cells were washed with cold PBS and lysed in urea lysis buffer containing 20 mM HEPES pH 8.0, 8 M urea and protease and phosphatase inhibitor mixture tablets (Roche, Indianapolis, IN). Cells were sonicated three times on ice using a Branson 250 sonicator (Hampton, NH) at 20% pulse for 30 s. The samples were then centrifuged at 20,000 × g for 15 min at 15 °C and the protein concentration of the supernatant was measured *via* a modified Lowry assay (BioRad, Hercules, CA).

2.2. Protease digestion, peptide clean-up and IP-enrichment of phosphotyrosine peptides

Lysates prepared in urea buffer from were reduced by 4.5 mM dithiothreitol (DTT) solution at 60 °C for 20 min. This was followed by cysteine alkylation by 10 mM iodoacetamide (IAA) for 15 min in the dark. The samples were diluted four-fold to a final concentration of 2 M urea, 20 mM HEPES pH 8.0 and subsequently digested with trypsin (Worthington, Lakewood, NJ) at a ratio of 1:100 (trypsin: protein, w/w) for 16 h at 30 °C. The digests were then acidified to a final concentration of 1% trifluoroacetic acid (TFA) to quench the protease digestion. The digested peptides were desalted using a solid-phase extraction C18 column (40 μm, 1 g, Supelco, Bellefonte, PA). The desalted peptides were lyophilized and stored at −80 °C until further use. The endogenous phosphotyrosine peptides were enriched using a PhosphoScan Kit with modified antibodies (combination of pY100 and pY1000 antibody slurries, 1:1 v/v, Cell Signaling, Danvers, MA). For each sample, a total of 8 mg digested protein extract was suspended in IAP buffer (50 mM MOPS, pH 7.2, 10 mM sodium phosphate, 50 mM NaCl) and incubated with 80 μL of the immobilized anti-Tyrosine antibody for 2 h at 4 °C. After incubation, the antibody bound beads were centrifuged for 30 s at 2000 × *g* and the supernatant was pipetted out and stored. The antibody beads were then washed twice with 1 mL IAP buffer and once with 1 mL chilled water. The phosphotyrosine peptides were eluted off the antibody beads by incubating twice with 55 μL of 0.15% TFA in water at room temperature for 10 min and mixing gently and intermittently. The eluted phosphopeptides were desalted using Pierce C18 spin tips (Thermo Scientific, Rockford, IL).

2.3. Synthetic peptide standards

The initial development of MRM assays was carried out using heavy isotope-labelled synthetic peptides with a C-terminal ^{15}N- and ^{13}C-labelled arginine ($^{13}C_6$, $^{15}N_4$) or lysine ($^{13}C_6$, $^{15}N_2$) residues, resulting in a mass shift of +10 or +8 Da, respectively. Unlabeled $^{12}C_6$ (light) versions of the peptides were also synthesized and used as internal standards for building the calibration curves. These were purchased from New England Peptides Inc. (+ 95% purity by HPLC, Gardner, MA). The peptides were quantified by amino acid analysis by the company, aliquoted and stored at −80 °C until use.

2.4. Nano-LC-MRM method development and analysis

For assay development, the synthetic peptides were reconstituted in 0.1% formic acid and were analyzed on a nano-chip-LC using a 1260 Infinity Series HPLC-Chip cube interface

(Agilent, Palo Alto, CA) coupled to a 6495-triple quadrupole mass spectrometer (Agilent, Palo Alto, CA). A large capacity chip system (G4240-62010) consisting of a 160 nL enrichment column and a 150 mm × 75 μm i.d. analytical column (Zorbax 300SB-C18, 5 μm, 300 Å pore size) was used. Mobile phase A consisted of 95% water, 4.9% acetonitrile and 0.1% FA, and mobile phase B consisted of 95% acetonitrile, 4.9% water with 0.1% FA. A flow rate of 3 μL/min was applied for sample loading by the capillary pump and 600 nL/min for the analytical separation through the nano pump. A 25-minute linear gradient (0 min, 0% B, 1 min, 5% B; 17 min, 40% B; 20 min, 70% B; 21 min, 80% B; 25 min 0% B) was used for the chromatographic separation of the target peptides. An electrospray ionization voltage of 1850 V was applied and quadrupoles 1 and 3 were run at 0.7 *m/z* FWHM resolution.

Individual injections were carried out to select transitions (defined as fragmentation of a precursor into a specific product ion for a given peptide). The optimum transitions were selected based on the presence of the top 5 most intense y-ions at *m/z* greater than the precursor *m/z*, to minimize crosstalk from potential interfering transitions occurring from singly charged precursor ions. When there were no y-ions present at a *m/z* greater than the precursor, then other more abundant b- and y-ions were chosen. The raw data were imported into Skyline 3.7 [28] and manually reviewed to delete transitions with interferences. The MRM assay for each peptide consisted of two to five transitions. The collision energies were calculated by Skyline for the monoisotopic precursor and product masses for the Agilent 6495 system. An equation, CE = 0.04 × *m/z* + y-intercept was used, and intercepts of −5.5664 and −4.8 were applied for doubly and triply charged precursors, respectively (CE = collision energy, *m/z* = mass to charge ratio of the precursor ion). The optimum transitions were combined in one scheduled MRM method with a 25-min run time and 2-min retention time windows, using retention times extracted during the MRM assay refinement stage. To minimize carryover, calibration samples were run from lower to higher concentrations and two blank injections were performed in between each sample injection. The sample carryover amount was estimated by determining the percentage intensity in the second blank compared to the sample intensities.

2.5. MRM assay refinement, generation of calibration curves and statistical data analysis

The initial development of the MRM assays was carried out using stable-isotope labelled standards to select optimum transitions. The synthetic peptide standards were reconstituted in 0.1% formic acid, pooled and used for method optimization. A spectral library (Fig. 1, [29]) was generated with our discovery data [21] to help select these transitions. All the raw data files were imported into Skyline 3.7 and data annotations were manually inspected. For endogenous target peptide identifications, we required that all the monitored transitions had nearly identical elution profiles, as well as good correlation with the relative transition intensities of the spiked-in internal standards, which were defined by ratio dot-product (rdotp) values, and that the observed elution times were consistent with the hydrophobicity of the peptides (Fig. 2, DIB manuscript). We used SSRCalc 3.0 [30] to predict retention times of the targets for the scheduled method building.

The synthetic peptides were spiked in the samples right before LC-MRM analysis. Peak area ratios (PAR) of isotopically normal (*i.e.* light) endogenous signals to isotopically enriched (*i.e.* heavy) internal standards were exported to Microsoft Excel for calculation of means, standard deviations and coefficients of variation. The generation of linear regression was carried out by building a reverse calibration curve [31] from H1975 DMSO treated lysates, trypsin digested, and phosphopeptide immunoprecipitated using the combination of pY100 and pY1000 antibodies (matrix-matching). Within the matrix of unlabeled endogenous tyrosine phosphorylated tryptic peptides, the amount of the heavy labelled standard was varied over a range (0.01, 0.1, 0.5, 2, 8, 50, 100, 500, 100 fmol) and a constant amount of the light peptide (2 fmol) was used as an internal standard. Linear regression was used to fit the data points using a 1/y weighting for each calibration standard. Coefficient of variation was used to determine the precision. The standard deviations (y-axis) of the three lowest calibrators (x-axis) were plotted and used to calculate the limits of detection (LOD) and lower limits of quantification (LOQ) for each peptide, where LOD = 3 × y-intercept and LOQ = 10 × y-intercept of those plots [32].

Quantitation was carried out by comparing the cells following TKI treatment to the controls using a two-tailed *t*-test (p-values < 0.05 were considered statistically significant). To identify differentially phosphorylated phosphotyrosine peptides, the mean PAR was used for relative quantitation. The endogenous abundance of the targets was estimated by the amounts calculated from the linear regression obtained from the calibration curves.

2.6. cBioPortal analysis

The TCGA lung adenocarcinoma dataset that consisted of the maximum number of sequenced cases (520 patients) was interrogated through the cBioPortal [33,34] for alterations in our gene list (Table 1) for missense, truncating and in-frame mutations, amplification and deletions, mRNA up- and downregulation and protein up- and down regulation by RPPA assay. Most of these were early stage lung cancer patients who underwent surgery. A survival analysis was also carried out comparing the cases with alterations in our query list to the ones without alterations to look at the median disease-free survival.

3. Results

The overall goal of this study was to develop modified immuno-MRM-based quantitative assays to detect and quantify tyrosine phosphorylation on specific tyrosine phosphorylated peptides of key signaling proteins involved in lung cancer-specific mutant EGFR signaling. The peptides selected for this study were identified in our previous SILAC-based quantitative DDA (Data Dependent Acquisition) studies [19–21] (Table 1). Phosphorylation at these sites was higher in cells expressing mutant EGFRs and/or inhibited upon treatment with 1st and 2nd generation EGFR TKIs, erlotinib and afatinib, respectively, in TKI-sensitive but not TKI-resistant lung adenocarcinoma cells.

3.1. LC-MRM method development and optimization

For each peptide target, two to five MRM transitions were chosen to build the optimized MRM assays for targeted proteomics. We synthesized these peptides with heavy amino acid-labelled Arg or Lys at the C-terminus and first, determined the optimal chromatographic separation of the target peptides (Fig. 1A). Chromatographic co-elution of the target endogenous peptides with the stable-isotope labelled internal standards was required for the highest confidence of detection (Fig. 1B). All the target peptides had rdotp values of over 0.9, thereby indicating confident identifications in the biological samples. For quantitation, noisy transitions and transitions with co-eluting interferences were discarded. The final method after the refinement stage consisted of 12 peptides comprising 87 transitions (Table 1, [29]).

The SSRCalc linear regression was used for retention time prediction for scheduling the MRM assays (Fig. 2, [29]). Given the average chromatographic peak width was around 30 s, a cycle time of 1.3 s for the scheduled methods allowed for sufficient sampling across the chromatographic peak. For any given peptide, the single transition that was free of interfering co-eluting ions and had good signal intensity was chosen as the “quantifier” for the quantitative assay while the remaining transitions were used as “qualifiers” to allow for maximum specificity. At any given time during the scheduled method, the dwell time varied from 80 to 160 milliseconds with 8 to 16 concurrent transitions being measured in any specified retention time window (Fig. 4A and B, [29]). The resulting scheduled MRM methods with a 120 s window allowed for over 20 points across the chromatographic peak for the “quantifier” transitions for all of the peptide targets. The scheduled MRM method resulted in superior chromatographic profiles for the final assays showing clearly defined peak areas for endogenous peptides and the heavy labelled standards in both H3255 experiments (Fig. 2) and H1975 experiments (Fig. 5, [29]).

We tested our standardized assays to interrogate changes in tyrosine phosphorylation in EGFR TKI-sensitive cell line H3255, and TKI-resistant cell line H1975, upon treatment with the 1st generation EGFR TKI, erlotinib and the 3rd generation EGFR TKI, osimertinib. Erlotinib is expected to inhibit phosphorylation of these targets in H3255, but not in H1975, since these cells are resistant to erlotinib. In contrast, osimertinib is expected to inhibit phosphorylation of these targets in both H3255 and H1975 cells. Tyrosine phosphorylated peptides were enriched using anti-phosphotyrosine (pY) antibodies. To optimize the enrichment of the phospho-tyrosine peptides, a combination of two pY antibodies, pY100 and pY1000 were used. Analysis of the enriched phosphopeptides by DDA-based LC-MS/MS using the two antibodies showed on average, an overlap of ~60% of the enriched peptides (Fig. 3A and B, Supplementary Table 1 in [29]). Hence, a combination of the two antibodies was used for the enrichment of pY peptides. The median retention time CVs among the three process replicates for H1975 DMSO/vehicle treated cells was 0.28% for the endogenous peptides and 0.23% for the heavy-labelled peptides (Fig. 3A). All the monitored transitions for each peptide co-eluted. The phoshotyrosine target ERRFI1-pY394 was not chosen for further optimizations owing to poor stability of the heavy labelled standard. The peak area ratios (PAR) were calculated by normalizing the peak intensity of the endogenous peptide transitions to that of the heavy labelled standard peptide. The CV values for the

PARs for the three process replicates in H1975 DMSO/vehicle treated cells ranged from 13.9% to 56.4% with a median CV of 27.47% (Fig. 3B).

3.2. Relative quantitation of the phosphotyrosine sites upon TKI treatment in the lung adenocarcinoma cells

The quantitative analysis of tyrosine phosphorylation of the peptides was carried out using three to six biological replicates for the controls and the TKI treated cells (Supplementary Table 1). The average of the median PAR CVs for the "quantifier" ion across three biological replicates of the targets analyzed upon DMSO/vehicle, erlotinib and osimertinib treatment was 26.7% (range 17–35%) in H3255 experiments (Fig. 6A, [29]) and 26.29% (range 19.2–35.5%) in H1975 experiments (Fig. 6B, [29]). The drug sensitive cells, H3255, showed significant downregulation of phosphorylation for all the phosphotyrosine sites with p-values < 0.005 (Fig. 4A). In H1975 cells, there was no statistically significant change in the tyrosine phosphorylation of the targets upon erlotinib treatment. The MRM ratios of phosphorylation at AHNAK-pY715, DAPP1-pY139 and CAV1-pY14 were < 0.5, but these changes were not statistically significant ($p > 0.05$) (Supplementary Fig. 1). In contrast, relative quantitation showed that the treatment with osimertinib in these cells led to statistically significant downregulation of STAT5A-pY694 (p-value = .0006) and EGFR-pY1197 (p-value = 0.004) over six biological replicates and CAV1-pY14 (p-value = 0.02) over three biological replicates (Fig. 4B). Unsupervised clustering analysis of the $\log_2$-transformed MRM ratios of erlotinib and osimertinib showed that the H3255 experiments clustered together and so did the H1975 experiments. EGFR-pY1197, pY1172 and STAT5A-pY694 clustered together (Fig. 5).

3.3. Phosphopeptide abundance estimation using calibration curves

After examining the relative changes in phosphorylation, we wanted to more precisely quantify the tyrosine phosphorylated peptides in these cell lines upon erlotinib or osimertinib treatment. Quantitation of the phosphopeptides as measured by the MRM assays does not account for the changes in the protein levels. However, our previous studies show that short-term (1-hour) TKI treatments do not alter the protein abundances. Development of similar immuno-MRM assays for protein estimations may be needed to provide insight into the stoichiometric changes.

In order to characterize the analytical performance of the quantitative assays, we built the response curves in digested and phosphotyrosine enriched matrix of H1975 cells treated with DMSO and processed in the same fashion as the TKI treated samples (Fig. 7, [29]). A reverse curve approach was used to eliminate the interferences from the endogenous signals and to estimate the figures of merit like method dynamic range, limit of detection (LOD) and limit of quantification (LOQ). Our matrix-matched external multi-point calibration curves were linear over 2–4 orders of magnitude. Precision was excellent with replicate CVs under 20%. Of all the chosen targets, EGFR-pY1172 did not show a linear response to the dilution series, while the remaining peptide curves were linear with $R^2 > 0.9$ (Table 2).

In H3255 cells, the abundance of phosphorylated EGFR peptides containing EGFR-pY998 and -pY1197 phosphosites reduced significantly from around 60 fmol/mg lysate to around

5fmol/mg lysate, consistent with our results from relative quantification (Fig. 6A). Although the amounts determined for the DMSO-treated sample by the linear regression were above the linear dynamic range, the drug treatments showed a significant downregulation in the tyrosine phosphorylations of these sites, indicating the inhibitory effects of the TKIs. In these cells, the abundance of EGFR-pY998-containing peptide was downregulated by 13.4-fold and 11.8-fold by osimertinib and erlotinib, respectively. Also, the abundance of EGFR-pY1197-containing peptide was downregulated by 15-fold and 18.3-fold by osimertinib and erlotinib, respectively. On the other hand, for the 1st generation TKI resistant H1975 cells, the abundance of EGFR-pY998 was upregulated with drug treatments (erlotinib treatment, average amount = 4.38 fmol/mg, p-value = 0.03 and osimertinib treatment, average amount = 3.73 fmol/mg, p-value = 0.1). EGFR-pY1197 peptide abundance was not significantly altered upon erlotinib treatment, but was significantly reduced upon osimertinib treatment (p-value = 0.009) (Fig. 6B).

The average abundance of INPPL1-pY1135-containing peptide in DMSO treated H3255 cells was 1.08 fmol/mg. Upon either TKI treatment, the amounts significantly reduced (osimertinib treatment, p-value = 0.0002 and erlotinib treatment, p-value = 0.0004) compared to control DMSO treatment (Fig. 6A). However, since the values of abundance upon TKI treatment were under the LOD, this phosphopeptide could not be reliably quantified. The levels of INPPL1-pY1135-containing peptide in H1975 cells in all conditions were at LOD levels. Hence reliable quantitation could not be carried out for this phosphopeptide for H1975 cells.

The abundance value of AHNAK-pY160-containing peptide in H3255 was significantly lower upon both erlotinib (1.5-fold downregulation, p-value = 0.009) and osimertinib treatment (1.5-fold downregulation, p-value = 0.001) (Fig. 6A) while the levels of AHNAK-pY160 in H1975 cells was not significantly altered upon either of the TKI treatments. The quantification for the remainder of sites was unreliable as the amounts calculated fell outside the domain of their respective standard curves (Supplementary Fig. 2).

4. Discussion

Kinase domain mutations in EGFR have been used to predict response to treatment with EGFR TKIs in lung adenocarcinoma patients. Accordingly, FDA has approved companion diagnostics for several of these mutations to select patients to be treated with different generations of EGFR TKIs. However, the partial response rates (> 30% of shrinkage of tumors using RECIST criteria) are in the range of 70–80% with different generations of EGFR TKIs for treatment of newly diagnosed patients and even falls to around 60–70% in patients who have developed resistance to 1st or 2nd generation EGFR TKIs and harbor the most common TKI-resistant mutation, T790 M. Here, we developed modified immuno-MRM assays for enrichment of tyrosine phosphorylated peptides using a combination of pY100 and pY1000 antibodies, and carried out the quantitation of tyrosine phosphorylation of specific phosphopeptides of key mutant EGFR signaling proteins. These phosphosites exhibited increased phosphorylation in human bronchial epithelial cells expressing mutant EGFRs. In addition, phosphorylation at these sites was inhibited in human lung adenocarcinoma cells that were sensitive to 1st generation EGFR TKI, erlotinib, and 2nd

generation EGFR TKI, afatinib. We validated these assays in two lung adenocarcinoma cell lines with varying sensitivities to the 1st and 3rd generation EGFR TKIs, erlotinib and osimertinib respectively.

H3255 human lung adenocarcinoma cell line, harboring the EGFR TKI sensitizing mutation L858R is sensitive to both erlotinib and osimertinib. Osimertinib targets the TKI-sensitizing mutations (sensitive to 1st generation EGFR TKIs), as well as the most common acquired resistance mutation in EGFR, T790M. Recently, a large randomised double-blind phase 3 trial demonstrated that the median progression free survival was longer with osimertinib than with the 1st generation EGFR TKIs, gefitnib or erlotinib, in newly diagnosed patients with EGFR mutations [35]. Treatment of H3255 with erlotinib or osimertinib represents “front-line” treatment of patients in this published study. Relative quantification carried out by comparing PARs through our validated MRM assays showed that tyrosine phosphorylation of the phosphopeptides chosen for this study was inhibited significantly ($p < 0.005$) upon treatment with either erlotinib or osimertinib in H3255 cells. Tyrosine phosphorylation of CAV1-pY14 was inhibited with erlotinib, but was not significant in this cell line. This is likely due to a lower endogenous level of CAV1 protein itself in H3255. The chromatographic peak for this phosphopeptide had low intensity in control lysates with DMSO treatment and was at background levels upon drug treatment in H3255. The hypophosphorylation of EGFR-pY998, EGFR-pY1197, INPPL1-pY1135, AHNAK-pY160, STAT5A-pY694 and NEDD9-pY164 phosphosites upon both TKI treatments was verified through the reverse calibration curves as well.

On the other hand, H1975 lung adenocarcinoma cells harboring the EGFR L858R and T790M mutations are resistant to erlotinib, but are sensitive to osimertinib. Accordingly, there was no significant decrease in tyrosine phosphorylation of our chosen phosphosites upon erlotinib treatment in these cells. However, relative quantitation showed that osimertinib treatment significantly reduced tyrosine phosphorylation of EGFR-pY1197 (p-value = 0.009), STAT5A-pY694 (p-value = 0.02) and CAV1-pY14 (p-value = 0.01), suggesting that these phosphosites are indeed potential biomarkers of osimertinib sensitivity in these cells. However, we were only able to confirm the hypophosphorylation of EGFR-pY1197 by osimertinib through the calibration curve in these cells. Several of the targets were beyond the range of the calibration curve in these cells, hence the quantitation itself was not reliable (Supplementary Fig. 2). It is interesting that abundance of EGFR-pY998, although within the range of the calibration curve, did not reduce upon osimertinib treatment in these cells. EGFR-pY998 may be phosphorylated by tyrosine kinases other than EGFR and possibly osimertinib may not have an off-target effect on any of these kinases.

To the best of our knowledge, this is the first study that uses a pan-pTyr antibody to enrich and quantify endogenous phosphotyrosine peptides in an immuno-MRM assay. The modified immuno-MRM assays presented here represent a general approach to validate a set of potential phosphotyrosine peptides from a larger set of putative phosphopeptide biomarkers. One limitation of our study is that the PAR variability among biological replicates are relatively high for specific phosphopeptides. However, IMAC-based enrichment of pSer/Thr/Tyr phosphopeptides followed by MRM assays for quantitation also showed median CVs in the range of 6.5–24.5% for pSer/Thr/Tyr sites [36] and 19.2–29.3%

for pTyr sites across biological replicates [37] underscoring the fact that more global approaches to enrichment of phosphopeptides show higher CVs for quantitation. Although time consuming and relatively expensive, additional method development by carrying out enrichments through phosphosite-specific antibodies may be needed to decrease this variability and assay imprecision. One previous study demonstrated the feasibility of utilizing phosphosite-specific antibodies followed by MRM quantification. The authors showed median intra-assay and inter-assay variability of 10% and 16% respectively across process replicates [26].

One possible explanation of higher variability in TKI treated cells is significant and complete inhibition of downstream phosphorylation thereby producing the chromatographic peaks below the detection limits. Peaks with low signal to noise ratios may have poor integration and will therefore show higher variability. Moreover, we observe high biological variability of endogenous target phosphorylation in the control cells treated with DMSO. The higher variability of the endogenous phosphopeptide abundances without any TKI inhibition in the control cells may reflect culture conditions including confluence of cells, lysis conditions and phosphatase activities, among others.

Previously we have shown significant downregulation of EGFR-pY1197 in lung adenocarcinoma cells that harbor 1st and 2nd generation EGFR TKI-sensitizing EGFR mutations upon treatment with either erlotinib or afatinib. More importantly, the degree to which tyrosine phosphorylation was inhibited at this site was lower in 11–18 lung adenocarcinoma cells with lesser sensitivity to the these TKIs compared to H3255 cells, while both cell lines harbored the TKI sensitizing mutant $EGFR^{L858R}$ [21]. Here, we have further validated EGFR-pY1197 as a potential biomarker of TKI sensitivity by developing the pY1197 quantitative MRM assay. Interestingly, a quantitative phospho-tyrosine MS analysis combined with a partial least-squares regression (PLSR) analysis showed that EGFR-pY1197 and INPPL1-pY1135 were among the epidermal growth factor (EGF) and hepatocyte growth factor (HGF) network-specific markers of invasion in A549 lung adenocarcinoma cells that harbor the KRAS G12V mutation but wild type EGFR [38]. This suggests that the assays developed in this study may also be used in predicting the biology of even wild type EGFR-harboring NSCLC tumors.

STAT5A is constitutively activated downstream of *BCR-ABL, $JAK2^{V617F}$, FLT3-ITD* or $cKIT^{D816V}$ oncogenes in many hematological malignancies and myeloproliferative diseases [39]. Activated SRC family kinases (SFKs) in BCR-ABL expressing cells can interact with STAT5A, inhibit its dimerization, and phosphorylate STAT5A-pY694 leading to cytoplasmic localization of STAT5A [40]. It has been previously shown that the STAT5A-pY694 phosphorylation was inhibited by ruxolitinib, a JAK1/2 inhibitor in JAK2V617F cells that resulted in prevention of cell proliferation *in vitro* and effective control of myeloproliferation *in vivo* [41]. STAT5A-pY694 is also a downstream target of EGFRVIII mutation in glioblastoma [42]. Here, we show that STAT5A-pY694 is inhibited by both erlotinib and osimertinib in H3255 cells, but only by osimertinib in H1975 cells that are resistant to erlotinib, further demonstrating that this is indeed a mutant EGFR target and this site can be a novel biomarker of EGFR TKI response.

CAV1-pY14 phosphorylation and its specific interaction with extracellular matrix (ECM) proteins and integrins are required for melanoma cell migration and metastasis. However, mutated CAV1-Y14F did not affect the tumor suppressor function of CAV1 [43]. Another study showed the involvement of CAV1-pY14 in reinforcing the activation of ERK or AKT kinases and thereby leading to increased proliferation, migration, invasiveness and development of chemo-resistance in rhabdomyosarcoma (RMS). This study also showed that the reduction of the pY14 levels by Src-kinase inhibitors counteracted the malignant phenotype of RMS cells [44]. Y14 phosphorylated CAV1 functions as an effector of Rho/ROCK signaling in the focal adhesion turnover and in turn promotes cancer cell invasion and migration. A feedback loop was defined between Rho/ROCK, Src, CAV1-pY14 in metastatic tumor cell protrusions [45]. The crosstalk between Mgat5/galectin lattice and CAV1-pY14 was implicated in focal adhesions turnover due to the stabilization of focal adhesion kinases (FAKs), elucidating the inter-dependent roles of galectin-3 and CAV1-pY14 in cancer cell migration [46]. In our study, CAV1-pY14 phosphorylation was significantly inhibited by osimertinib, but not erlotinib, in H1975 cells, suggesting that mutant EGFRs directly or indirectly through other tyrosine kinases, such as SFKs, can phosphorylate CAV1 at Y14, and that the inhibition of this phosphorylation can predict TKI responsiveness.

We previously showed DAPP1-pY139 as a novel target of the mutant EGFRs. We also showed the involvement of DAPP1 in the survival of mutant EGFR-addicted cells [21]. Here, the DAPP1-pY139 MRM assay reproducibly showed significant inhibition of phosphorylation by both erlotinib and osimertinib in H3255 cells.

The MRM assays developed in this study to detect and quantify tyrosine phosphorylation of specific targets allow us to add another dimension to the investigation of specific alterations in genes promoting tumorigenesis. Upon querying the TCGA provisional database for lung adenocarcinoma, our results indicate that our target list was found to be altered in 292 (56%) of the total 520 patients sequenced (Fig. 7A). Interestingly, there was significantly lower disease-free survival among patients with combined alterations of our set of genes (Logrank test p-value: 0.0369) (Fig. 7B). Similar analysis on a subset TCGA dataset that is published [47] showed a better p-value in disease free survival (Logrank test *p*-value:0.006) (Fig. 8, [29]). However, with this limited retrospective data, we do not suggest that our list of phosphosites of mutant EGFR targets constitute a “signature” to predict survival of patients with lung adenocarcinoma. The MRM assays described in this study can be used to validate prospectively differential phosphorylation of our list of phosphosites in patients with EGFR mutant lung adenocarcinoma in the context of clinical trials. These assays can be used to interrogate phosphorylation levels of these peptide biomarkers in tumor biopsies or surgeries before EGFR TKI treatment and upon development of resistance to measure the levels of tyrosine phosphorylation and predict TKI response.

5. Conclusions

MRM-based proteomics is a powerful technique to verify potential biomarkers in complex samples with great selectivity. These assays routinely employ heavy labelled synthetic peptides for accurate quantification of the target endogenous peptides. In the present study,

we performed quantitative MRM using stable isotope labelled synthetic peptides and a global phosphotyrosine peptide enrichment strategy to characterize dynamic changes of phosphorylation downstream of mutant EGFRs in lung adenocarcinoma cells harboring $EGFR^{L858R}$ and $EGFR^{L858R/T790M}$, the TKI-sensitive, and TKI-resistant mutants, respectively. A list of targets was selected from our previous SILAC-based quantitative mass spectrometry studies. We further validated these sites as mutant EGFR targets, and the dynamics of tyrosine phosphorylation at these sites correlated well with TKI sensitivity of lung adenocarcinoma cells. Lung adenocarcinoma patients with alterations in genes selected in our study had poorer disease-free survival, as revealed from the TCGA data. We propose that alteration in tyrosine phosphorylation, as demonstrated by our modified immuno-MRM assays, will better predict disease prognosis as well as treatment response, and will add a new dimension to correlation of gene alteration with patient survival.

The MRM proteomics data in this paper have been deposited in the Peptide Atlas [48] database with a dataset identifier PASS01129.

Supplementary Material

Refer to Web version on PubMed Central for supplementary material.

Acknowledgements

This research was supported by the Intramural Research Program of the NIH, Center for Cancer Research, National Cancer Institute (U.G.) (ZIABC011410).

References

[1]. Siegel RL, Miller KD, Jemal A, Cancer statistics, 2017, CA Cancer J. Clin 67 (1) (2017) 7–30. [PubMed: 28055103]

[2]. Zhang X, et al., An allosteric mechanism for activation of the kinase domain of epidermal growth factor receptor, Cell 125 (6) (2006) 1137–1149. [PubMed: 16777603]

[3]. Lynch TJ, et al., Activating mutations in the epidermal growth factor receptor underlying responsiveness of non-small-cell lung cancer to gefitinib, N. Engl. J. Med 350 (21) (2004) 2129–2139. [PubMed: 15118073]

[4]. Paez JG, et al., EGFR mutations in lung cancer: correlation with clinical response to gefitinib therapy, Science 304 (5676) (2004) 1497–1500. [PubMed: 15118125]

[5]. Pao W, Miller VA, Kris MG, 'Targeting' the epidermal growth factor receptor tyrosine kinase with gefitinib (Iressa®) in non-small cell lung cancer (NSCLC), Semin. Cancer Biol 14 (1) (2004) 33–40. [PubMed: 14757534]

[6]. Dowell J, Minna JD, Kirkpatrick P, Erlotinib hydrochloride, Nat. Rev. Drug Discov 4 (1) (2005) 13–14. [PubMed: 15690599]

[7]. Pao W, et al., EGF receptor gene mutations are common in lung cancers from "never smokers" and are associated with sensitivity of tumors to gefitinib and erlotinib, Proc. Natl. Acad. Sci. U. S. A 101 (36) (2004) 13306–13311. [PubMed: 15329413]

[8]. Copeman M, Prolonged response to first-line erlotinib for advanced lung adenocarcinoma, J. Exp. Clin. Cancer Res 27 (1) (2008) 59. [PubMed: 18983643]

[9]. Kobayashi S, et al., EGFR mutation and resistance of non-small-cell lung cancer to gefitinib, N. Engl. J. Med 352 (8) (2005) 786–792. [PubMed: 15728811]

[10]. Pao W, et al., Acquired resistance of lung adenocarcinomas to gefitinib or erlotinib is associated with a second mutation in the EGFR kinase domain, PLoS Med. 2 (3) (2005) e73. [PubMed: 15737014]

[11]. Bean J, et al., MET amplification occurs with or without T790M mutations in EGFR mutant lung tumors with acquired resistance to gefitinib or erlotinib, Proc. Natl. Acad. Sci. U. S. A 104 (52) (2007) 20932–20937. [PubMed: 18093943]

[12]. Engelman JA, et al., MET amplification leads to gefitinib resistance in lung cancer by activating ERBB3 signaling, Science 316 (5827) (2007) 1039–1043. [PubMed: 17463250]

[13]. Turke AB, et al., Preexistence and clonal selection of MET amplification in EGFR mutant NSCLC, Cancer Cell 17 (1) (2010) 77–88. [PubMed: 20129249]

[14]. Suda K, et al., Small cell lung cancer transformation and T790M mutation: complimentary roles in acquired resistance to kinase inhibitors in lung cancer, Sci. Rep 5 (2015) 14447. [PubMed: 26400668]

[15]. Niederst MJ, et al., RB loss in resistant EGFR mutant lung adenocarcinomas that transform to small-cell lung cancer, Nat. Commun 6 (2015) 6377. [PubMed: 25758528]

[16]. Maemondo M, et al., Gefitinib or chemotherapy for non–small-cell lung cancer with mutated EGFR, N. Engl. J. Med 362 (25) (2010) 2380–2388. [PubMed: 20573926]

[17]. Rosell R, et al., Erlotinib versus standard chemotherapy as first-line treatment for European patients with advanced EGFR mutation-positive non-small-cell lung cancer (EURTAC): a multicentre, open-label, randomised phase 3 trial, Lancet Oncol. 13 (3) (2012) 239–246. [PubMed: 22285168]

[18]. Wu YL, et al., Afatinib versus cisplatin plus gemcitabine for first-line treatment of Asian patients with advanced non-small-cell lung cancer harbouring EGFR mutations (LUX-Lung 6): an open-label, randomised phase 3 trial, Lancet Oncol. 15 (2) (2014) 213–222. [PubMed: 24439929]

[19]. Guha U, et al., Comparisons of tyrosine phosphorylated proteins in cells expressing lung cancer-specific alleles of EGFR and KRAS, Proc. Natl. Acad. Sci. U. S. A 105 (37) (2008) 14112–14117. [PubMed: 18776048]

[20]. Zhang X, et al., Identifying novel targets of oncogenic EGF receptor signaling in lung cancer through global phosphoproteomics, Proteomics 15 (2–3) (2015) 340–355. [PubMed: 25404012]

[21]. Zhang X, et al., Quantitative tyrosine Phosphoproteomics of epidermal growth factor receptor (EGFR) tyrosine kinase inhibitor-treated lung adenocarcinoma cells reveals potential novel biomarkers of therapeutic response, Mol. Cell. Proteomics 16 (5) (2017) 891–910. [PubMed: 28331001]

[22]. Wolf-Yadlin A, et al., Multiple reaction monitoring for robust quantitative proteomic analysis of cellular signaling networks, Proc. Natl. Acad. Sci 104 (14) (2007) 5860–5865. [PubMed: 17389395]

[23]. de Graaf EL, et al., Signal transduction reaction monitoring deciphers site-specific PI3K-mTOR/MAPK pathway dynamics in oncogene-induced senescence, J. Proteome Res 14 (7) (2015) 2906–2914. [PubMed: 26011226]

[24]. Whiteaker JR, et al., Peptide immunoaffinity enrichment with targeted mass spectrometry: application to quantification of ATM kinase phospho-signaling, in: Kozlov SV (Ed.), ATM Kinase: Methods and Protocols, Springer New York, New York, NY, 2017, pp. 197–213.

[25]. Anderson NL, et al., Mass spectrometric quantitation of peptides and proteins using stable isotope standards and capture by anti-peptide antibodies (SISCAPA), J. Proteome Res 3 (2) (2004) 235–244. [PubMed: 15113099]

[26]. Whiteaker JR, et al., Peptide immunoaffinity enrichment and targeted mass spectrometry enables multiplex, quantitative pharmacodynamic studies of phospho-signaling, Mol. Cell. Proteomics 14 (8) (2015) 2261–2273. [PubMed: 25987412]

[27]. Jänne PA, et al., AZD9291 in EGFR inhibitor–resistant non–small-cell lung cancer, N. Engl. J. Med 372 (18) (2015) 1689–1699. [PubMed: 25923549]

[28]. MacLean B, et al., Skyline: an open source document editor for creating and analyzing targeted proteomics experiments, Bioinformatics 26 (7) (2010) 966–968. [PubMed: 20147306]

[29]. Awasthi S, et al., Dataset describing the development, optimization and application of SRM/MRM based targeted proteomics strategy for quantification of potential biomarkers of EGFR TKI sensitivity. 10.1016/j.dib.2018.04.086 (Epub ahead of print)

[30]. Krokhin OV, Sequence-specific retention calculator. Algorithm for peptide retention prediction in ion-pair RP-HPLC: application to 300- and 100-A pore size C18 sorbents, Anal. Chem 78 (22) (2006) 7785–7795. [PubMed: 17105172]

[31]. Campbell J, et al., Evaluation of absolute peptide quantitation strategies using selected reaction monitoring, Proteomics 11 (6) (2011) 1148–1152. [PubMed: 21365756]

[32]. Anderson DJ, Determination of the lower limit of detection, Clin. Chem 35 (10) (1989) 2152–2153. [PubMed: 2619804]

[33]. Gao J, et al., Integrative analysis of complex cancer genomics and clinical profiles using the cBioPortal, Sci. Signal 6 (269) (2013) pl1. [PubMed: 23550210]

[34]. Cerami E, et al., The cBio cancer genomics portal: an open platform for exploring multidimensional cancer genomics data, Cancer Discov. 2 (5) (2012) 401–404. [PubMed: 22588877]

[35]. Soria J-C, et al., Osimertinib in untreated EGFR-mutated advanced non–small-cell lung cancer, N. Engl. J. Med 378 (2) (2017) 113–125. [PubMed: 29151359]

[36]. Mertins P, et al., Ischemia in tumors induces early and sustained phosphorylation changes in stress kinase pathways but does not affect global protein levels, Mol. Cell. Proteomics 13 (7) (2014) 1690–1704. [PubMed: 24719451]

[37]. Kennedy JJ, et al., Immobilized metal affinity chromatography coupled to multiple reaction monitoring enables reproducible quantification of phospho-signaling, Mol. Cell. Proteomics 15 (2) (2016) 726–739. [PubMed: 26621847]

[38]. Johnson H, et al., Phosphotyrosine profiling of NSCLC cells in response to EGF and HGF reveals network specific mediators of invasion, J. Proteome Res 12 (4) (2013) 1856–1867. [PubMed: 23438512]

[39]. Benekli M, et al., Signal transducer and activator of transcription proteins in leukemias, Blood 101 (8) (2003) 2940–2954. [PubMed: 12480704]

[40]. Fahrenkamp D, et al., Src family kinases interfere with dimerization of STAT5A through a phosphotyrosine-SH2 domain interaction, Cell Commun. Signal 13 (2015) 10. [PubMed: 25885255]

[41]. Bartalucci N, et al., Inhibitors of the PI3K/mTOR pathway prevent STAT5 phosphorylation in JAK2V617F mutated cells through PP2A/CIP2A axis, Oncotarget 8 (57) (2017) 96710–96724. [PubMed: 29228564]

[42]. Chumbalkar V, et al., Analysis of phosphotyrosine signaling in glioblastoma identifies STAT5 as a novel downstream target of ΔEGFR, J. Proteome Res 10 (3) (2011) 1343–1352. [PubMed: 21214269]

[43]. Ortiz R, et al., Extracellular matrix-specific Caveolin-1 phosphorylation on tyrosine 14 is linked to augmented melanoma metastasis but not tumorigenesis, Oncotarget 7 (26) (2016) 40571–40593. [PubMed: 27259249]

[44]. Faggi F, et al., Phosphocaveolin-1 enforces tumor growth and chemoresistance in rhabdomyosarcoma, PLoS One 9 (1) (2014) e84618. [PubMed: 24427291]

[45]. Joshi B, et al., Phosphorylated caveolin-1 regulates Rho/ROCK-dependent focal adhesion dynamics and tumor cell migration and invasion, Cancer Res. 68 (20) (2008) 8210–8220. [PubMed: 18922892]

[46]. Goetz JG, et al., Concerted regulation of focal adhesion dynamics by galectin-3 and tyrosine-phosphorylated caveolin-1, J. Cell Biol 180 (6) (2008) 1261–1275. [PubMed: 18347068]

[47]. The Cancer Genome Atlas Research, N, Comprehensive molecular profiling of lung adenocarcinoma, Nature 511 (2014) 543. [PubMed: 25079552]

[48]. Desiere F, et al., The PeptideAtlas project, Nucleic Acids Res. 34 (Suppl. 1) (2006) D655–D658. [PubMed: 16381952]

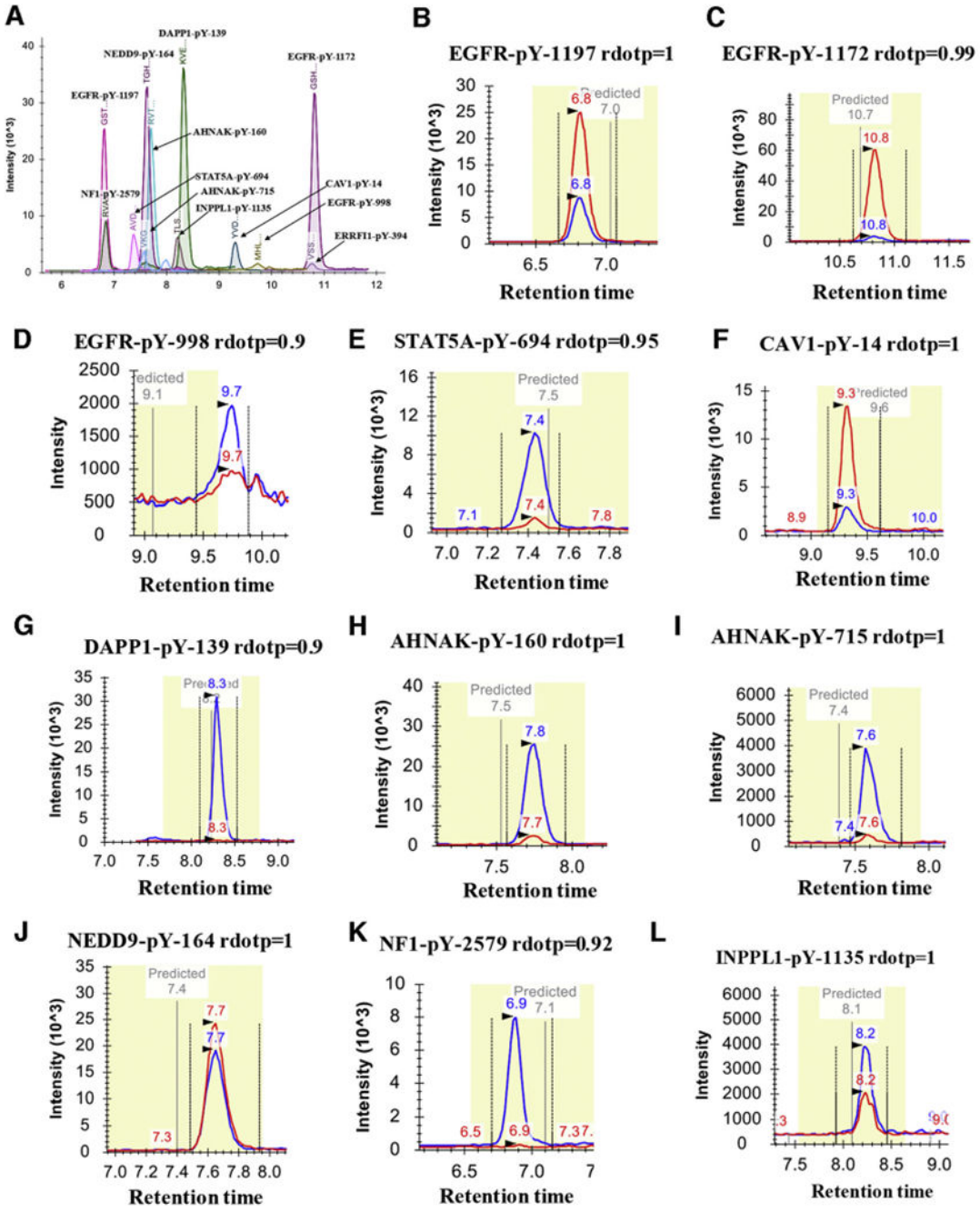

Fig. 1.

Optimized chromatographic separation of the target phosphopeptides from method development stage. A) The final scheduled method showing the elution of the targets with 2-min retention time windows in DMSO/vehicle treated H1975 cells. B–L) The representative chromatograms for each target is marked by a black arrow. The red peak represents the endogenous peptide chromatogram and the blue is the heavy labelled internal standard spiked-in at a constant amount of 2 fmol in all samples. The grey bars are the predicted retention times from SSRCalc 3.0. rdotp represents the correlation between the endogenous

and internal standard chromatograms. (For interpretation of the references to colour in this figure legend, the reader is referred to the web version of this article.)

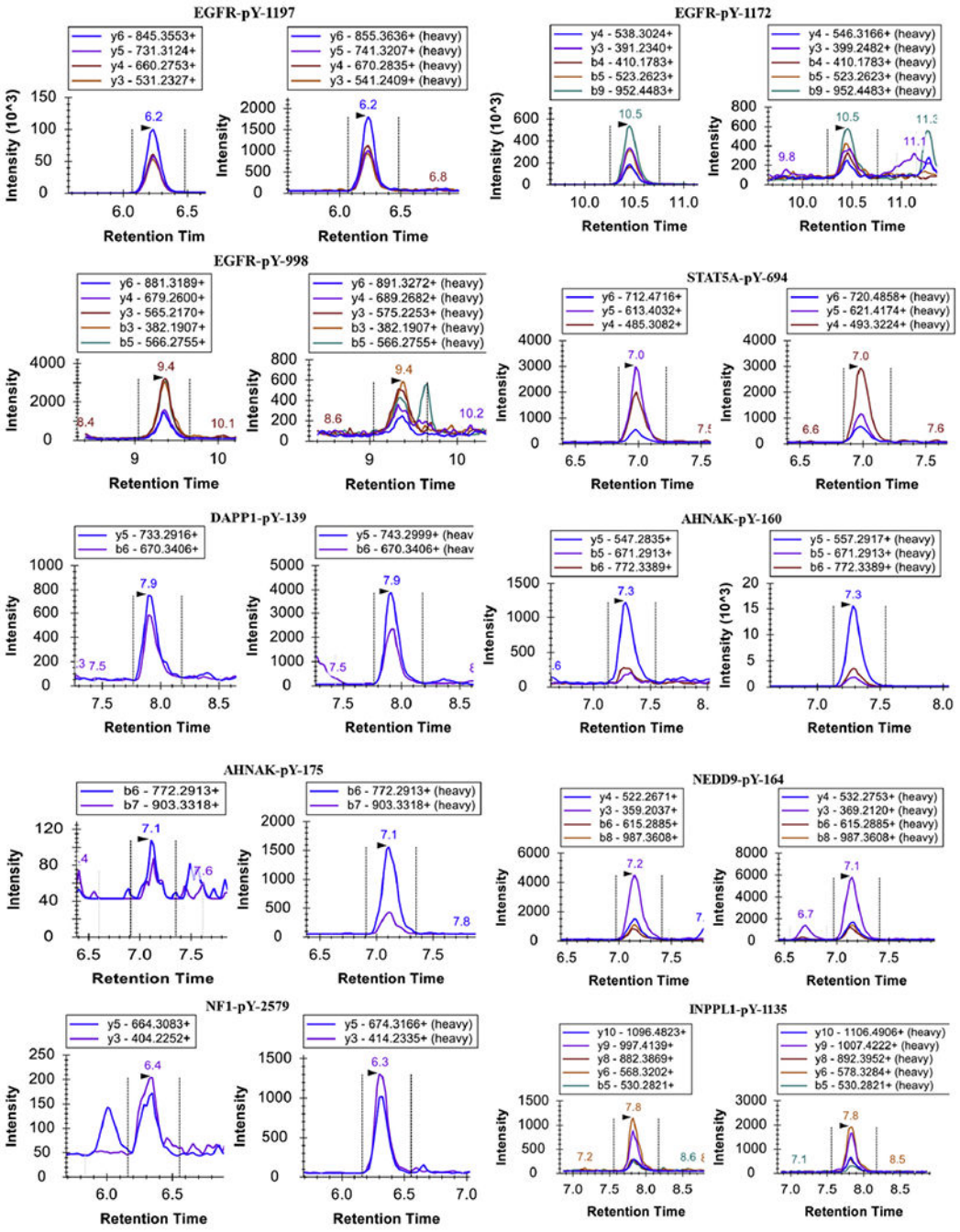

Fig. 2.

Chromatographic profile for the endogenous (left) and the heavy labelled internal standards (right) for H3255 (DMSO/vehicle treated) cells.

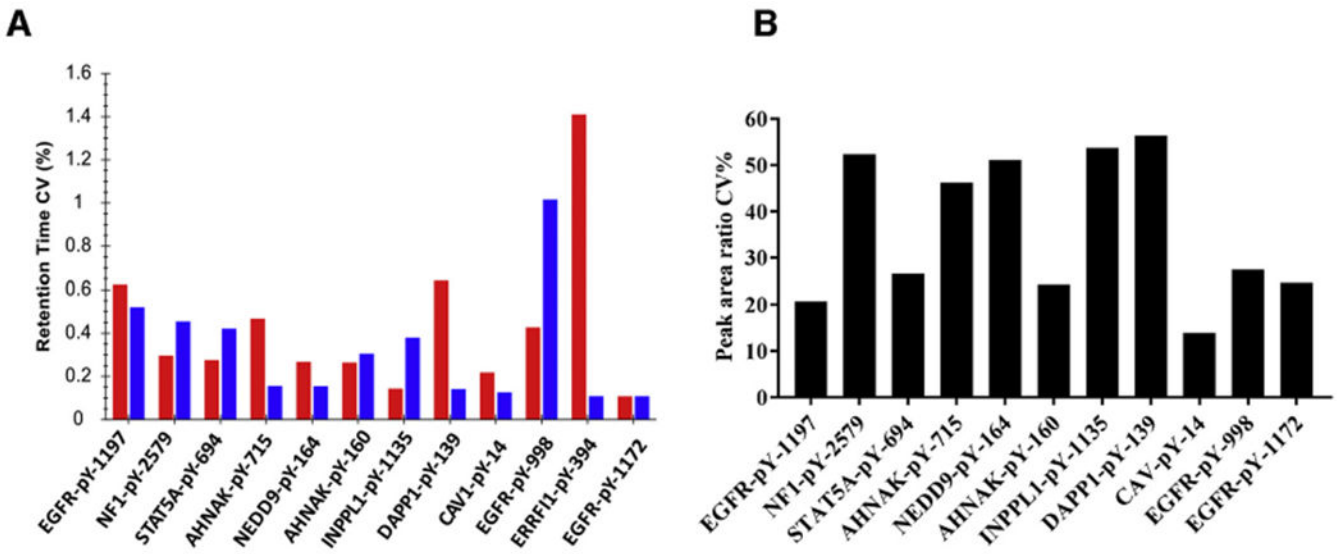

Fig. 3.

Reproducibility of the optimized MRM assays from three independent proteolytic digestions and immunoprecipitations of DMSO/vehicle treated H1975 cells. A) Retention time repeatability; the red and blue bars represent endogenous and internal standard peptides, respectively. The median CV was 0.28% for the endogenous peptides and 0.23% for the internal standards. B) Peak area ratios as determined by normalizing the signal intensities of the endogenous to the internal standards. The median CV was 27.47%. (For interpretation of the references to colour in this figure legend, the reader is referred to the web version of this article.)

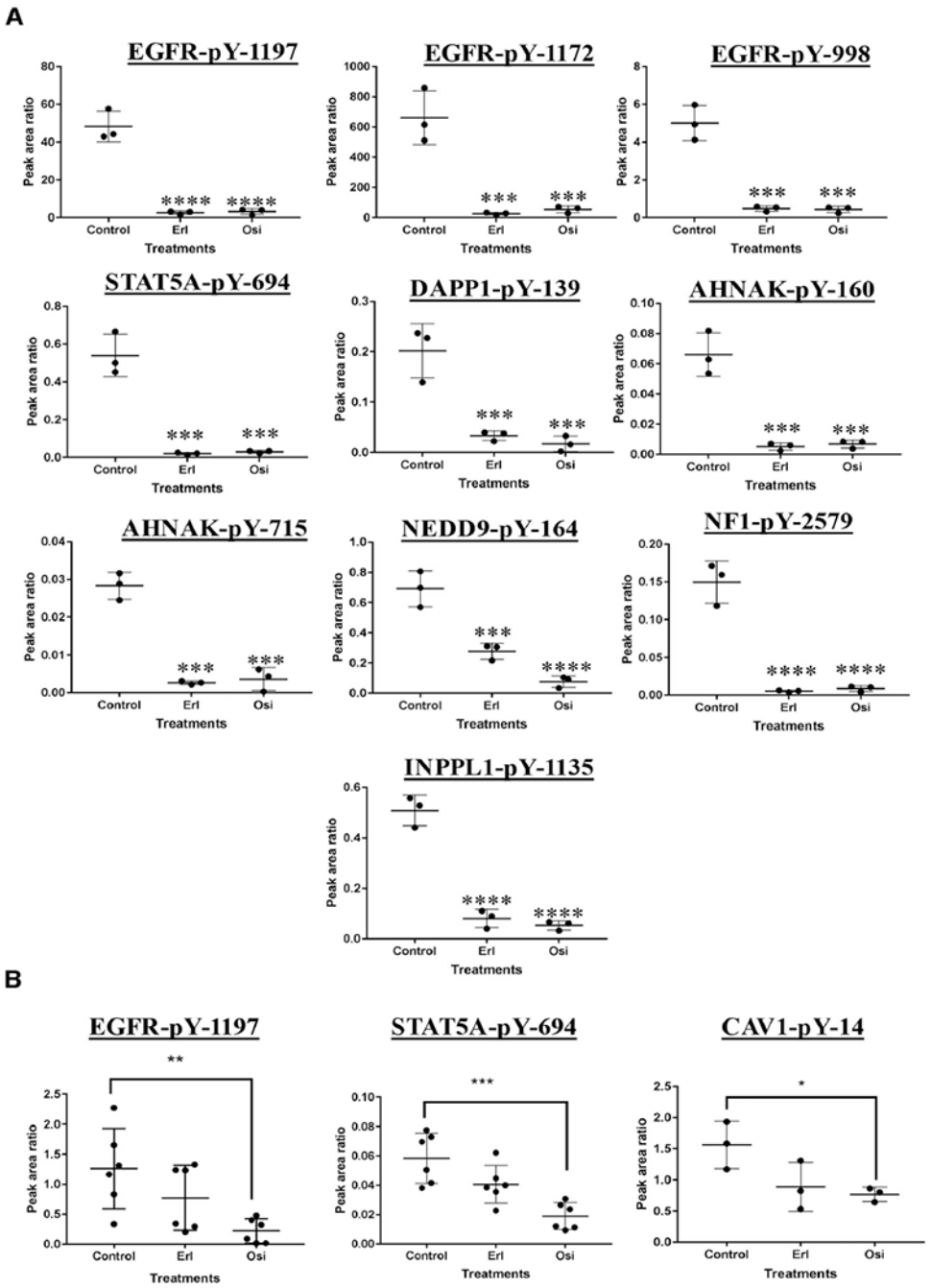

Fig. 4.

Relative quantitation of phosphopeptides using peak area ratios. A) All the phosphotyrosine sites were significantly downregulated ($p < 0.005$) in drug sensitive H3255 cells upon treatments with erlotinib (Erl) and osimertinib (Osi). B) Phosphotyrosine sites EGFR-pY1197, STAT5A-pY694 and CAV1-pY14 in the H1975 cells show significant hypophosphorylation ($p < 0.05$) with osimertinib, but not with erlotinib treatment (n.s. - not significant).

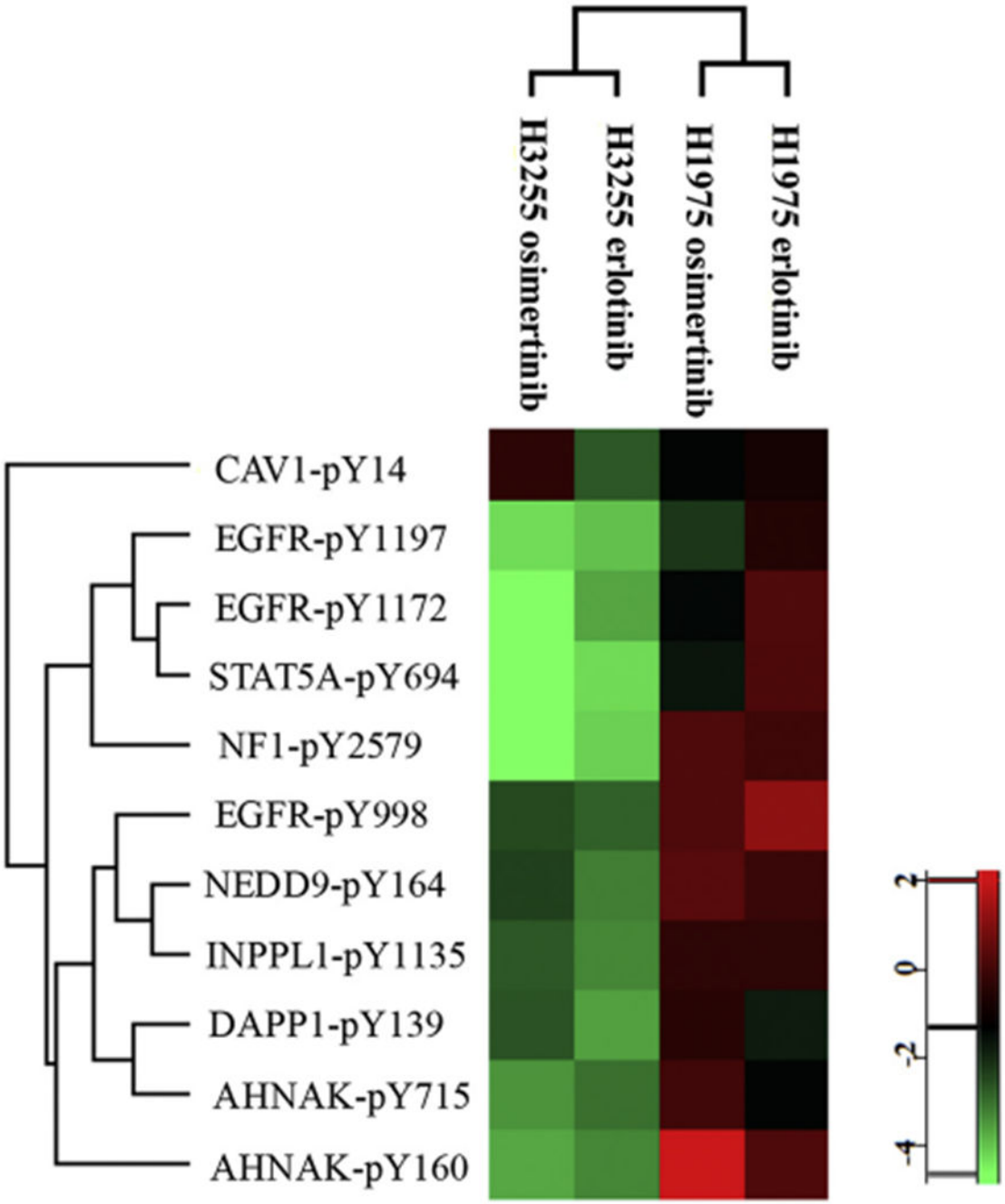

Fig. 5.

Unsupervised hierarchical clustering of the peak area ratios from relative quantitation of phosphorylation of the targets. Heat map shows the average $\log_2$ transformed MRM ratios for erlotinib and osimertinib treatments from three biological replicates in H3255 and H1975 cells.

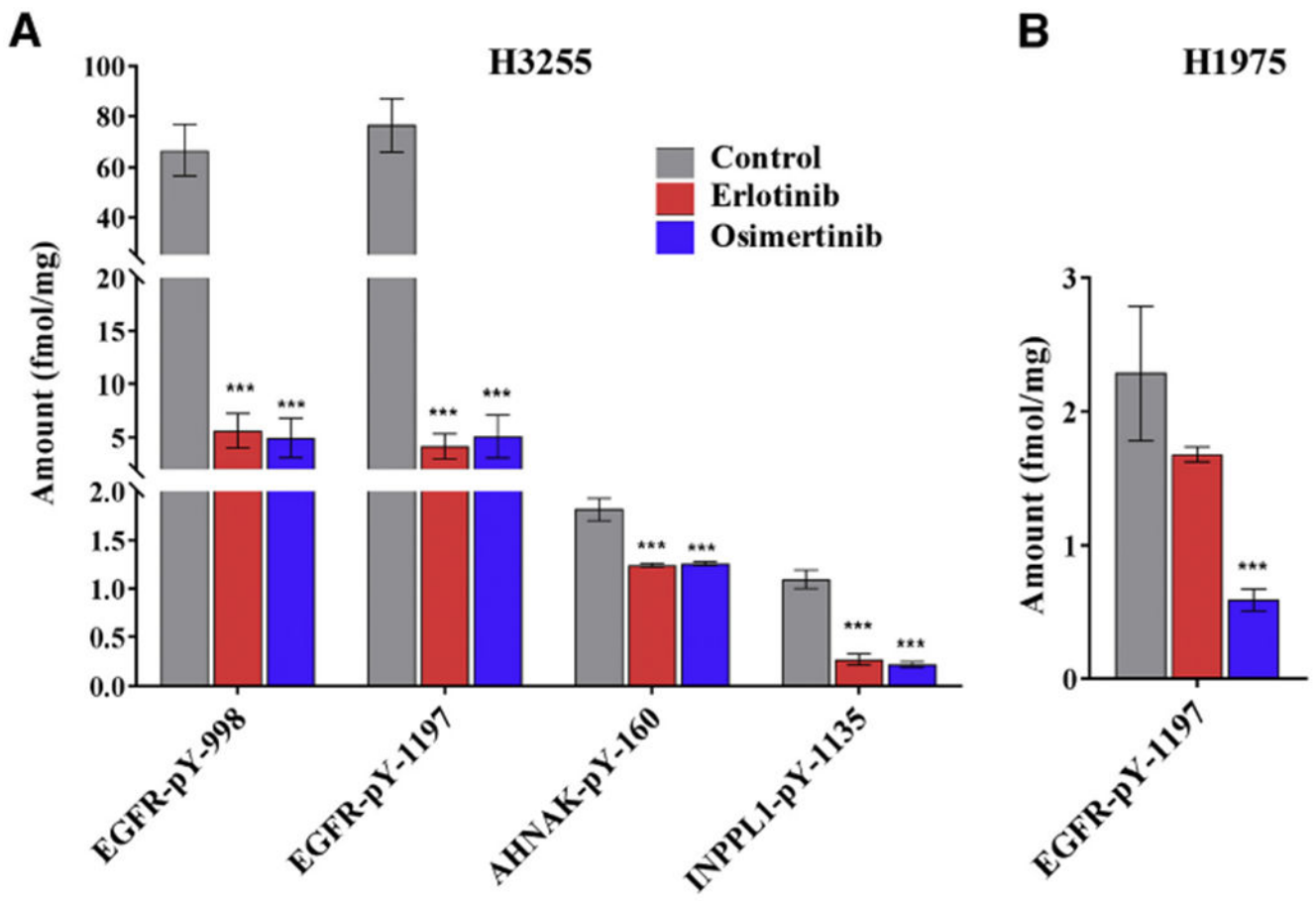

Fig. 6.

Bar charts showing the quantitative data of phosphopeptide abundance obtained with and without TKI treatments from three biological replicates in A) H3255 and B) H1975 cells. Error bars are ± standard deviations.

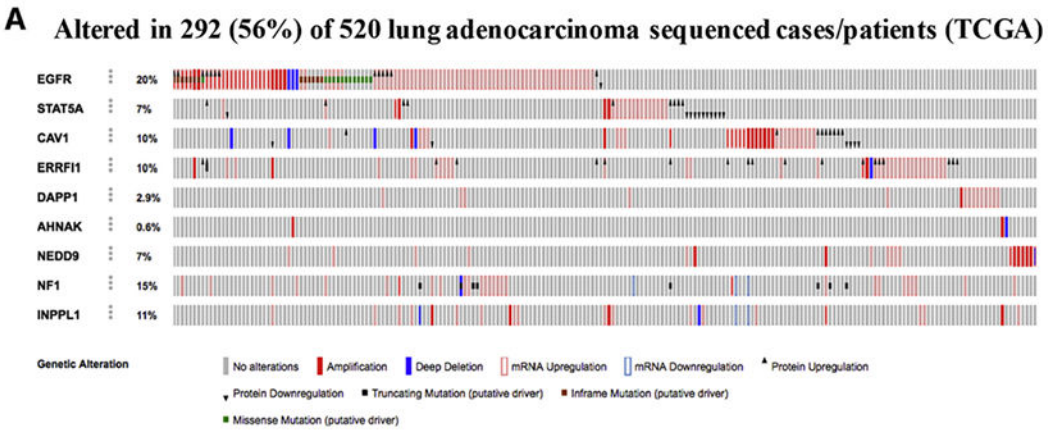

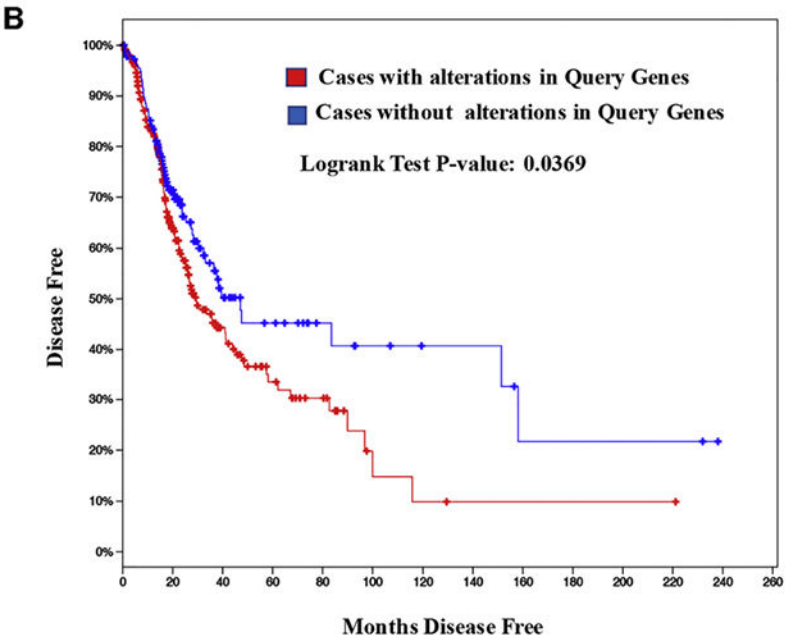

	Total cases	Cases relapsed	Disease free survival (median months)
Cases with Alterations in Query Genes	251	119	29.5
Cases without Alterations in Query Genes	184	68	47.08

Fig. 7.

cBioPortal query of the TCGA lung adenocarcinoma dataset for alterations in genes of the list of targets and correlation with disease-free survival. A) Combined alterations of 9 genes for our assay targets were seen in 292 cases (56%) of lung adenocarcinoma in the TCGA dataset, and B) patients with alterations in our genes had a statistically significant lower disease-free survival when compared to cases with no alterations.

Table 1

The list of phosphotyrosine tryptic peptide targets used for the development of the modified immuno-MRM assays.

Protein names	Gene names	Targets	Sequence
Epidermal growth factor receptor	EGFR	Y-998	MHLPSPTDSNFY(P)R
		Y-1172	GSHQISLDNPDY(P)QQDFFPK
		Y-1197	GSTAENAEY(P)LR
Signal transducer and activator of transcription 5A	STAT5A	Y-694	AVDGY(P)VKPQIK
Caveolin-1	CAV1	Y-14	YVDSEGHLY(P)TVPIR
ERBB receptor feedback inhibitor 1	ERRFI1	Y-394	VSSTHY(P)YLLPERPPYLDK
Dual adapter for phosphotyrosine and 3-phosphotyrosine and 3-phosphoinositide	DAPP1	Y-139	KVEEPSIY(P)ESVR
Neuroblast differentiation-associated protein	AHNAK	Y-160	RVTAY(P)TVDVTGR
		Y-715	VKGEY(P)DMTVPK
Enhancer of filamentation 1	NEDD9	Y-164	TGHGYVY(P)EYPSR
Neurofibromin	NF1	Y-2579	RVAETDY(P)EMETQR
Phosphatidylinositol 3,4,5-trisphosphate 5-phosphatase 2	INPPL1	Y-1135	TLSEVDY(P)APAGPAR

J Proteomics. Author manuscript; available in PMC 2021 March 22.

Table 2

Phosphopeptide abundance determined from three biological replicates using calibration curves. Mean abundance of target phospho-peptides expressed in fmol/mg protein obtained from reverse calibration curves following treatment with DMSO/vehicle, erlotinib and osimertinib in H3255 and H1975 cells. LOD, Limit of Detection, LOQ, Limit of Quantification.

Gene names	Targets	R2	LOD	LOQ	Mean amount (fmol/mg)					
					H3255 (EGFR L858R)			H1975 (EGFR L858R/T790M)		
					Control	Erlotinib treatment	Osimertinib treatment	Control	Erlotinib treatment	Osimertinib treatment
EGFR	Y-998	0.91	0.27	0.9	66.65[c]	5.64	4.97	1.63	4.38	3.73
	Y-1197	0.97	0.195	0.65	76.51[c]	4.18	5.11	2.28	1.68	0.59[a]
AHNAK	Y-160	0.98	0.38	1.25	1.83	1.25	1.26	1.73	1.48	1.45
INPPL1	Y-1135	0.9	0.3	1.0	1.08	0.28[a]	0.22[a]	0.35[b]	0.3[b]	0.31[b]

[a]Under LOD.

[b]Under LOQ.

[c]Above linear dynamic range.